Flow and Axial Dispersion Simulation for Traveling Axisymmetric Taylor Vortices

Tony Howes
Dept. of Chemical Engineering, University of Queensland, St. Lucia, Queensland 4072, Australia

Murray Rudman
Commonwealth Scientific and Industrial Research Organisation (CSIRO), Division of Building, Construction and Engineering, P.O. Box 56, Highett, Victoria 3190, Australia

Numerical experiments using a finite difference method were carried out to determine the motion of axisymmetric Taylor vortices for narrow-gap Taylor vortex flow. When a pressure gradient is imposed on the flow the vortices are observed to move with an axial speed of 1.16 $\pm$ 0.005 times the mean axial flow velocity.

The method of Brenner was used to calculate the long-time axial spread of material in the flow. For flows where there is no pressure gradient, the axial dispersion scales with the square root of the molecular diffusion, in agreement with the results of Rosenbluth et al. for high Peclet number dispersion in spatially periodic flows with a roll structure. When a pressure gradient is imposed, the dispersion increases by an amount approximately equal to $6.5 \times 10^{-4}\ \overline{W}^2 d^2/D_m$, where $\overline{W}$ is the average axial velocity in the annulus, analogous to Taylor dispersion for laminar flow in an empty tube.

Introduction

Taylor (1923) studied the stability of the flow induced in a cylindrical annulus when the inner cylinder rotates. He found that when the rotation rate exceeds a critical value, pairs of counterrotating toroidal vortices appear that are regularly spaced in the axial direction. For the case where the gap-width in the annulus, d, is much less than the inner cylinder radius, R_i, the critical rotation rate corresponds to a Taylor number, $Ta = \omega^2 R_i d^3/\nu^2$, of 1708. Figure 1 shows the geometry of this flow.

When a small constant axial flow is added to the Taylor flow, axial motion of the vortices results, with little intermixing between neighboring vortices and efficient mixing within an individual vortex cell. This flow system may behave as a near-ideal plug-flow reactor, with consequent benefits (Kataoka et al. 1975; Kataoka and Takigawa, 1981). Radial and circumferential mixing is relatively fast, and the basic picture of the flow is that of individual, well-mixed vortices moving through the system.

Flow regimes for single-phase Taylor vortex flow are well studied, and mixing, dispersion, and heat/mass transport are fairly well understood. Pudjiono et al. (1992) describe applications for this flow, including viscometry, characterization of shear-dependent rate processes, cooling of rotating electrical machinery, dynamic filtration and classification, electrolytic applications, and catalytic chemical reactors.

A number of studies have been made on the stability of Taylor vortices in the presence of an axial flow. The two major results of these studies have been the discoveries that the critical Taylor number required to form vortices increases when there is a superimposed axial flow, and that at this critical Taylor number, the wavelength of the vorticies is less than the wavelength at critical Taylor number in the absence of an axial flow.

Chandrasekhar (1960) and DiPrima (1960) studied theoretically the effect of a superimposed axial flow by treating it as a constant average flow superimposed on the Couette and Taylor flows. They found that the vortices move with a velocity less than the average flow velocity, $\overline{W}$. The vortex velocity is the velocity at which the vortex centers are translated in the axial direction. Defining the axial flow Reynolds number, $Re_a = d\overline{W}/\nu$, Chandrasekhar (1962) calculated the stability in the limit as Re_a approaches zero, this time with the improved assumption that the superimposed axial flow has a parabolic profile. He found that the vortex velocity is 1.2 times the mean

Correspondence concerning this article should be addressed to T. Howes.

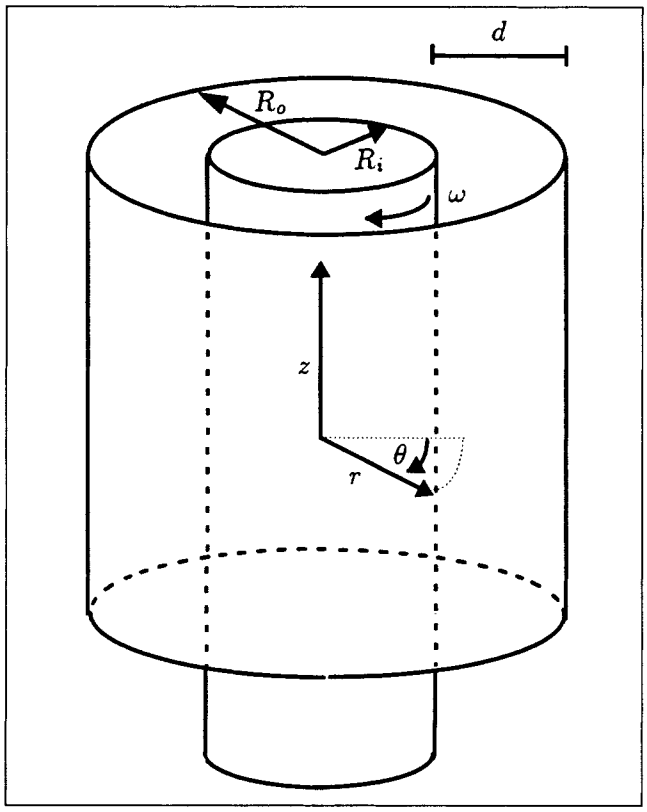

Figure 1. Taylor vortex flow geometry.

flow velocity and also derived a relationship between the critical Taylor number and axial flow Reynolds number. Datta (1965) corrected an error in the algebra of that article, which allows this relationship to be written correctly as $Ta_c = 1{,}708 + 1.32Re_a^2$. These results were experimentally verified by Snyder (1962), who found that the relationship between critical Taylor number and Re_a was accurate for $Re_a < 2$. Snyder observed that the flow remained axisymmetric for axial Reynolds numbers less than 20. Samson and Ayazi (1996) used tracer response curves and also found that the vortex velocity was approximately 1.2 times the axial flow velocity for a flow where $R_o/R_i = 1.18$, $Ta = 12{,}400$, and $Re_a = 12.5$. A good description of the history of this problem is given in DiPrima and Pridor (1979).

Bühler and Polifke (1990) found experimentally that toroidal vortices formed and traveled in the direction of the axial velocity. The size of the vortices was observed to be alternately large and small. For axial flow Reynolds numbers greater than 2.7, they found spiral wave solutions. In the narrow-gap limit, they also found that the linear theory predicts that axisymmetric vortices form that have a positive axial velocity proportional to the axial flow Reynolds number.

Gu and Fahidy (1985; 1986) experimentally showed that the effect of axial flow is to decrease wavelength and to increase critical Taylor number. Their range of axial flow Reynolds numbers is substantially higher than Snyder's, starting at $Re_a \approx 60$. Simmers and Coney (1980) used hot-wire anemometry to measure the radial variation in axial average velocity for a narrow gap with Re_a, and found that the core region of the flow moved axially with a velocity of 1.15 times the average fluid velocity.

Recently Moore and Cooney (1995) carried out a series of experiments in a flow-through Taylor–Couette vessel and measured dispersion for a wide range of geometries, rotation rates, and axial flow velocities. Their results suggest that axial dispersion is not dependent on molecular diffusivity and only weakly dependent on the axial flow Reynolds number, even for flow regimes known to be axisymmetric.

The difference between axial vortex velocity and mean axial flow velocity in the axisymmetric vortex regime is likely to influence axial dispersion. The current study aims at investigating the effect of an applied pressure gradient, and hence axial flow, on axial dispersion in this flow regime, and determining the functional relationship between dispersion, axial flow, and molecular diffusion for a single-cylinder geometry and rotation rate.

Numerical Methods

For axisymmetric swirling flow between two concentric cylinders, the Navier–Stokes equations for an incompressible, constant viscosity liquid can be written in cylindrical coordinates as,

$$\frac{1}{r}\frac{\partial(rU)}{\partial r} + \frac{\partial W}{\partial z} = 0, \tag{1}$$

$$\frac{\partial U}{\partial t} + \frac{1}{r}\frac{\partial(rU^2)}{\partial r} - \frac{V^2}{r} + \frac{\partial(WU)}{\partial z} = \frac{1}{Re}\left[\frac{\partial}{\partial r}\left(\frac{1}{r}\frac{\partial rU}{\partial r}\right) + \frac{\partial^2 U}{\partial z^2}\right] - \frac{\partial P}{\partial r}, \tag{2}$$

$$\frac{\partial V}{\partial t} + \frac{1}{r}\frac{\partial(rUV)}{\partial r} + \frac{UV}{r} + \frac{\partial(WV)}{\partial z} = \frac{1}{Re}\left[\frac{\partial}{\partial r}\left(\frac{1}{r}\frac{\partial rV}{\partial r}\right) + \frac{\partial^2 V}{\partial z^2}\right], \tag{3}$$

$$\frac{\partial W}{\partial t} + \frac{1}{r}\frac{\partial(rUW)}{\partial r} + \frac{\partial(W^2)}{\partial z} = \frac{1}{Re}\left[\frac{1}{r}\frac{\partial}{\partial r}\left(r\frac{\partial W}{\partial r}\right) + \frac{\partial^2 W}{\partial z^2}\right] - \frac{\partial P}{\partial z}. \tag{4}$$

Here U is the radial velocity (positive away from the center line), V is the azimuthal velocity (positive in an anticlockwise sense), and W is the axial velocity (positive upwards). Distance is scaled with the gapwidth d and velocity with ωR_i where ω is the angular velocity of the inner cylinder. Time is scaled with $d/(\omega R_i)$ and pressure with $\rho(\omega R_i)^2$. The Reynolds number is $Re = \omega d_{Ri}/\nu$, where ν is the kinematic viscosity.

Equations 1–4 are discretized on a uniform staggered cylindrical mesh, using the well-known MAC method (Welch et al., 1965). Grid pressures $P_{i,k}$ and azimuthal velocity components $V_{i,k}$ are defined at cell centers (i,k), and radial and axial velocity components are defined at the centers of cell faces, $U_{i+1/2,k}$ and $W_{i,k+1/2}$.

Advective fluxes are determined using a spatially third-order version of the QUICK scheme of Leonard (1979). Bilinear interpolation is used to obtain velocity components at

locations other than those at which they are defined. Although QUICK is stable, the QUICK fluxes are limited using a direction-split version of Zalesak's Flux-Corrected Transport (FCT) algorithm (Zalesak, 1979). Use of this flux-limiting procedure has been shown to considerably improve the monotonicity and accuracy of the solution (Li and Rudman, 1995). The low-order fluxes required in the limiting procedure are calculated using first-order up-winding. The viscous terms are discretized using second-order central differences, which makes the overall accuracy of the method second-order in space. The pressure solution is formulated using a projection method similar to that discussed in Amsden and Harlow (1970). The resulting Poisson equation for the pressure correction is solved using a defect-correction multigrid technique developed by Morton et al. (1995).

Temporal integration is accomplished using an (explicit) improved Euler step, and the method is thus second order in time. The additional computational expense involved in treating the diffusive terms with an implicit time discretisation was considered to be excessive for the time-dependent calculations undertaken here, and the time step is thus limited by the diffusive time-step criterion,

$$\delta t < \frac{Re\,\delta r^2 \delta z^2}{4(\delta r^2 + \delta r^2)}. \tag{5}$$

Given the values of $P^n_{i,k}$, $U^n_{i+1/2,k}$, $V^n_{i,k}$, and $W^n_{i,k+1/2}$, a simple first-order-in-time explicit update involves the following steps:

1. Find intermediate $(*)$ values of the $n+1$ velocity field based on old values of the pressure and velocities,

$$\boldsymbol{U}^* = \boldsymbol{U}^n + \delta t\left[-\nabla\cdot(\boldsymbol{U}\boldsymbol{U})^n + \frac{1}{Re}\nabla^2\boldsymbol{U}^n - \nabla P^n\right]. \tag{6}$$

2. Calculate the pressure correction δP for each grid cell (i,k) by solving the following Poisson equation:

$$\frac{1}{r}\frac{\partial}{\partial r}\left(r\frac{\partial \delta P}{\partial r}\right) + \frac{\partial^2 \delta P}{\partial z^2} = \frac{1}{\delta t}\left(\frac{1}{r}\frac{\partial (rU^*)}{\partial r} + \frac{\partial W^*}{\partial z}\right). \tag{7}$$

The source term on the righthand side of Eq. 7 is the divergence of the intermediate velocity field $\boldsymbol{U}^*$ divided by δt.

3. Correct the velocity and pressure fields,

$$\boldsymbol{U}^{n+1} = \boldsymbol{U}^* - \delta t \nabla \delta P \quad \text{and} \quad P^{n+1} = P^n + \delta P. \tag{8}$$

The improved Euler step used here involves two iterations of these three steps: the first iteration uses a half time-step to estimate velocities and pressures at $n+(1/2)$, and the second uses a full time-step with righthand side operators calculated using the $n+(1/2)$ velocities and pressures.

The multigrid technique employed here to solve the elliptic pressure correction equation (step 2) typically converges after an amount of work equivalent to 20–30 fine-grid successive overrelaxation (SOR) iterations irrespective of grid size.

Boundary conditions are implemented here identically to those in MAC. The outer cylinder is stationary and the inner cylinder rotates with a scaled azimuthal velocity $V=1$. Radial boundary conditions for pressure are not required (instead a zero normal-gradient condition is applied to the pressure correction). Axial boundary conditions for velocity are periodic. Axial boundary conditions for pressure are set to give a constant axial pressure gradient, $G = -\Delta P/L$, where L is the scaled axial length of the computational domain.

Initial conditions for simulations in which $G=0$ are obtained by superimposing a small perturbation on the cylindrical Couette flow solution,

$$V(r) = \frac{R'_o R'_i}{(R'_o + R'_i)}\left(\frac{R'_o}{r} - \frac{r}{R'_o}\right), \tag{9}$$

where R'_i and R'_o are the outer and inner radii scaled with the gap d. Provided the Taylor number is greater than 1708, the flow is unstable, and (axisymmetric) Taylor vortex flow results. For simulations where $G \neq 0$, the $G=0$ simulation is used as an initial condition but with an applied pressure gradient. Simulations were carried out on a uniform 64-by-128 grid, with the greater number of points in the axial direction. The axial extent of the domain was $L = 2.009$, which corresponds to the wavelength of the Taylor vortices at the critical Taylor number for $G=0$. In all cases, a single cell forms that contains a pair of counterrotating vortices.

Taylor Vortex Flow Patterns

All simulations discussed below were undertaken at $Ta = 3{,}125$, which is above the critical Taylor number, but below that at which an azimuthal mode becomes unstable and destroys the axisymmetry of the flow (Koschmeider, 1993). The ratio of gapwidth to inner radius is 1:20. Figure 2 shows

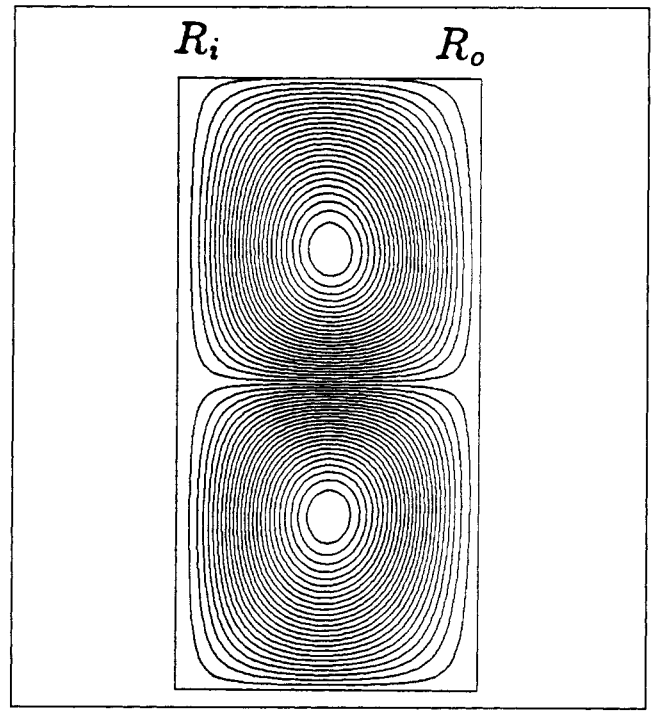

Figure 2. Stream function contour plot, $G=0$, $Ta=3125$, $R_o/R_i=1.05$.

stream function contours for the case where there is no applied pressure gradient. The righthand side of the figure is the outer cylinder wall and the lefthand side the inner cylinder wall. The figure shows the whole computational domain, and so represents one spatial period of the flow. This is the case for all of the plots showing stream function contours. In the figure, the upper vortex is rotating counterclockwise and the lower one clockwise. The maximum radial velocity was found to equal $0.05\omega R_i$ and the minimum radial velocity was $-0.0321\omega R_i$. Figure 2 shows the radial and axial motion—there is also an azimuthal component, V, which has not been shown, as it plays no part in the calculation of axial dispersion that follows. Figure 3 shows stream function contours for a flow with a pressure gradient, $G = 0.0005$. The central stream flow is upwards in the figures. The vortex velocity can be measured by looking at the stream function contour plot at a later time and measuring how far the vortex centers have traveled. From the distance of translation, the vortex velocity, $W_{vort} = 0.1217\omega R_i$, is calculated. The mean flow velocity, $\overline{W}$, is found by measuring the flow rate through the cell, and equals $0.01045\omega R_i$, corresponding to an axial Reynolds number, Re_a, of 2.61.

Figure 3 appears to suggest that the vortices are reduced in size as a result of the flow through and are separated by a large central meandering flow. This is fact is an illusion, as the flow from the viewpoint of a stationary observer is unsteady, and as a result pathlines are not the same as streamlines. In a coordinate frame moving with the vortex velocity, W_{vort}, the flow is steady. Figure 4 shows the stream function contour plot viewed in such a frame, for the same time as Figure 3. This shows that the basic Taylor cells have not changed greatly in structure from $G = 0$. Because the vortex train is moving upwards faster than the mean flow, in the moving frame there must be a flow of fluid downwards to ensure a balance of mass. The dotted contour lines in Figure 4 show this flow, which meanders around the vortices and along the cylinder walls. Figures 5 and 6 show the flow where G is increased to 0.001, where the vortex velocity is $0.0243\omega R_i$ and the mean axial velocity $0.0209\omega R_i$, corresponding to $Re_a = 5.25$. Again, the basic Taylor cells have not changed markedly, although the size of the counterflowing stream has grown. Values for $\overline{W}$ and W_{vort} have been measured for pressure gradients ranging from 10^{-4} to 10^{-3}, and are shown in Figure 7. The ratio $W_{vort}/\overline{W}$ ranges from 1.156 to 1.165, corresponding well with the results to Chandrasekhar (1962) and other numerical and experimental results.

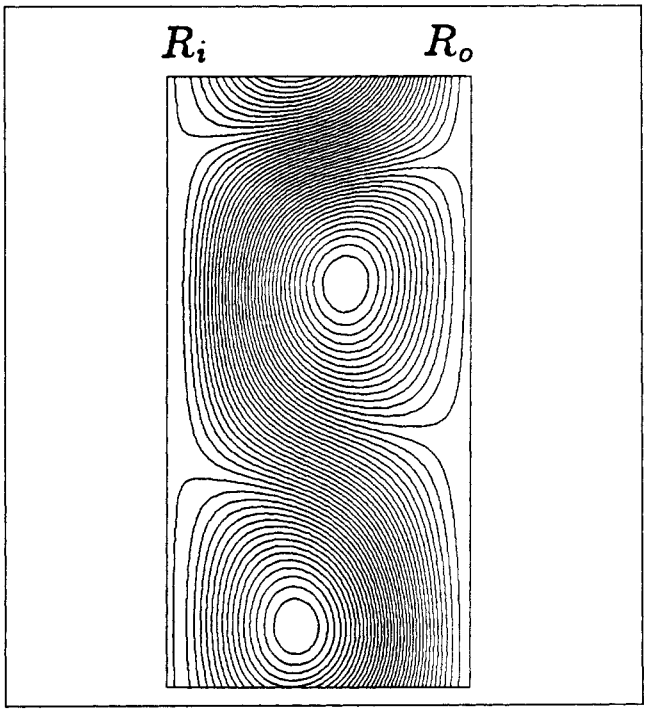

Figure 3. Instantaneous stream function contour plots, $G = 0.0005$, $Ta = 3{,}125$, $R_o/R_i = 1.05$.

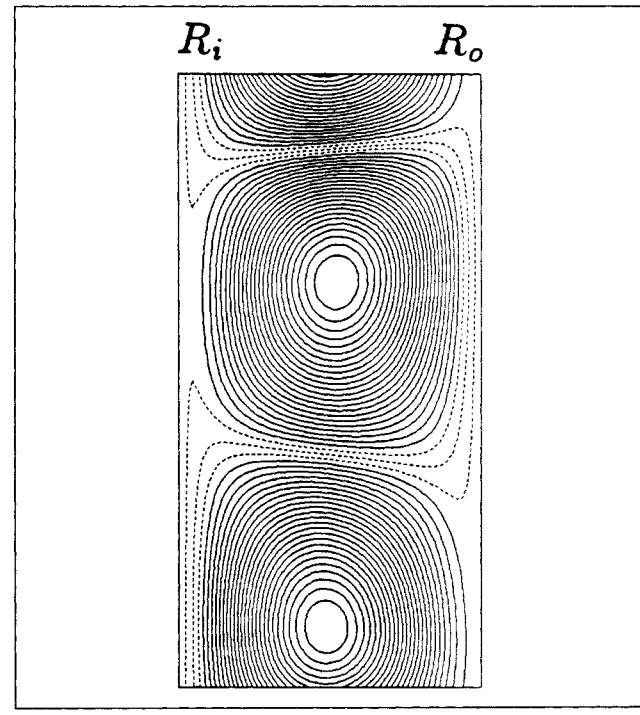

Figure 4. Instantaneous stream function contour plot in a frame moving with the vortex velocity, $W_{vort} = 0.01217$.

$G = 0.0005$, $Ta = 3125$, $R_o/R_i = 1.05$. The axial Reynolds number (Re_a) is 2.61.

Axial Dispersion

The method used to calculate the long-time axial dispersion of material is that first proposed by Brenner (1980) for general dispersion in spatially periodic material. In particular the formulation described by Carbonell and Whitaker (1983) is used below. These formulations have been developed for steady flow, so for our use the flows must be converted from flow in a stationary frame to flow in a frame moving with the vortex velocity by subtraction of W_{vort}.

The scaled axial dispersion, $\phi = D_a/(d\omega R_i)$, is found from

$$\phi = \langle W'f \rangle + \frac{1}{\sqrt{(TaR_i/d)Sc}}, \qquad (10)$$

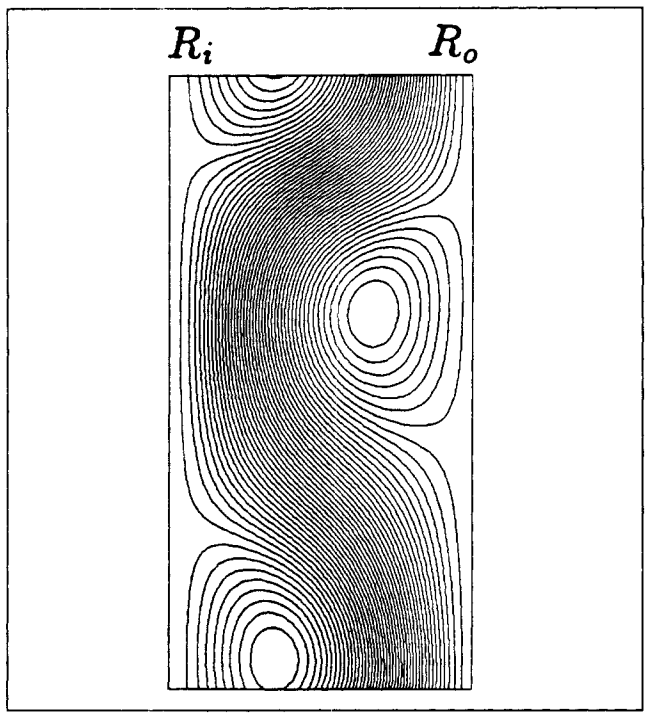

Figure 5. Instantaneous stream function contour plots, $G = 0.001$, $Ta = 3{,}125$, $R_o/R_i = 1.05$.

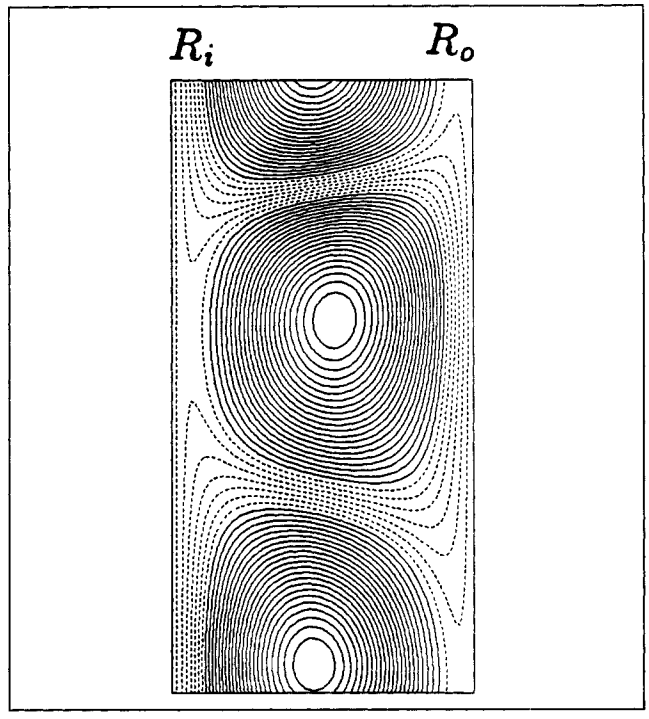

Figure 6. Instantaneous stream function contour plot in a frame moving with the vortex velocity, $W_{vort} = 0.0243$.

$G = 0.001$, $Ta = 3125$, $R_o/R_i = 1.05$. The axial Reynolds number (Re_a) is 5.25.

where $\langle\ \rangle$ represents the average over one spatial period of the flow and W' the deviation velocity, $W' = W - \langle W \rangle$. The function f satisfies

$$W' + \boldsymbol{U}\cdot\nabla f = \frac{1}{ReSc}\nabla^2 f, \tag{11}$$

subject to the boundary conditions,

$$f|_{z=L} = f|_{z=0}, \tag{12}$$

$$\left.\frac{\partial f}{\partial r}\right|_{r=R_i, r=R_o} = 0. \tag{13}$$

Equation 11 has been solved by finding the long-time solution of the transient convection-diffusion-like equation,

$$\frac{\partial f}{\partial t} = -W' - \boldsymbol{U}\cdot\nabla f + \frac{1}{ReSc}\nabla^2 f. \tag{14}$$

The QUICK scheme has been used for the advection term, and centered differences for the other terms. Calculation of f is undertaken on a finer grid (128×256) than that used to generate the velocities.

For Schmidt numbers (Sc) up to 100, the maximum difference between ϕ calculated on the 64×128 grid and that calculated on the 128×256 grid is 5%. However, the difference becomes larger as the Schmidt number increases, with differences of approximately 40% for $Sc = 1000$, showing the need for an even finer grid for high Schmidt number simulations.

Rosenbluth et al. (1987) have calculated the axial dispersion for a steady convective flow with a similar roll structure to Taylor–Couette flow. Defining a Peclet number, (Pe)

$$Pe = \hat{v}d_{\text{roll}}/D_m, \tag{15}$$

where $\hat{v}$ is a characteristic roll velocity, d_{roll} the axial extent of each roll $= \lambda/2$, and D_m is molecular diffusivity, it was found that in the limit of high Peclet number,

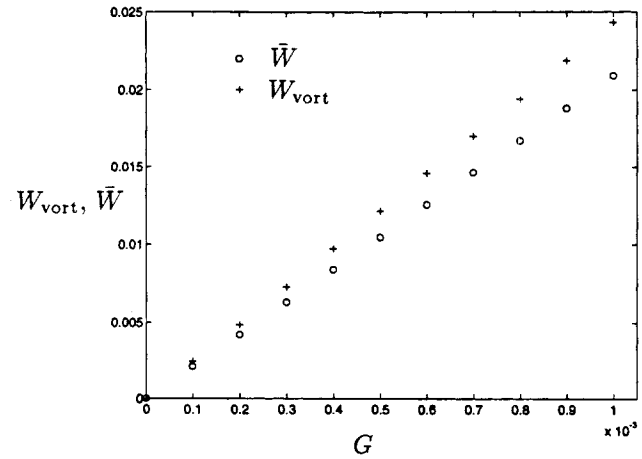

Figure 7. Vortex and mean axial flow velocity as a function of pressure gradient, $Ta = 3{,}125$, $R_o/R_i = 1.05$.

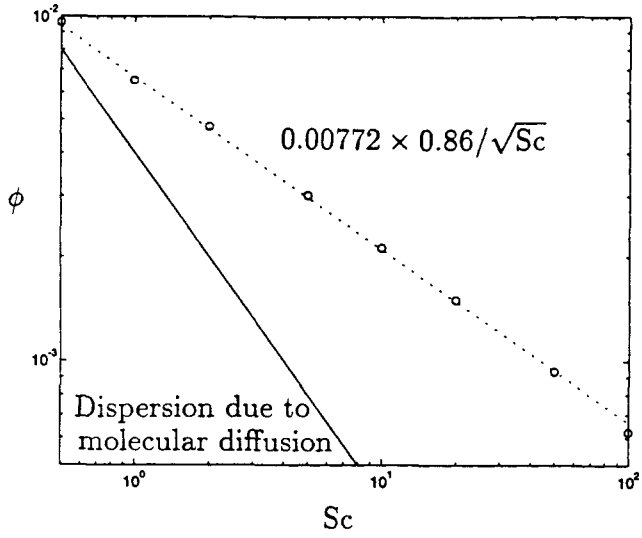

Figure 8. Axial dispersion vs. Schmidt number, $\bar{W} = 0$.

The dashed line shows the calculated dispersion using the analysis by Rosenbluth et al. (1987), with $\alpha = 0.86$. The solid line shows the dispersion due to molecular diffusion alone.

$$D_a = 0.6(D_m \hat{u} d_{\text{roll}} \beta)^{0.5} \alpha, \tag{16}$$

where α is $O(1)$ and geometry dependent, and β is the ratio of the axial extent of each roll to its radial extent—in this case $\beta = 1.0045$. Using the average of the magnitudes for the minimum and maximum radial velocity ($0.041\,\omega R_i$) as a value for $\hat{u}$, we find,

$$\phi_0 \approx 0.00772\,\alpha/\sqrt{Sc}\,. \tag{17}$$

Figure 8 shows the results for the calculated axial dispersion vs. Schmidt number for $G = 0$ and Sc ranging from 0.5 to 100. The best-fit curve through the points gives $\alpha = 0.86$.

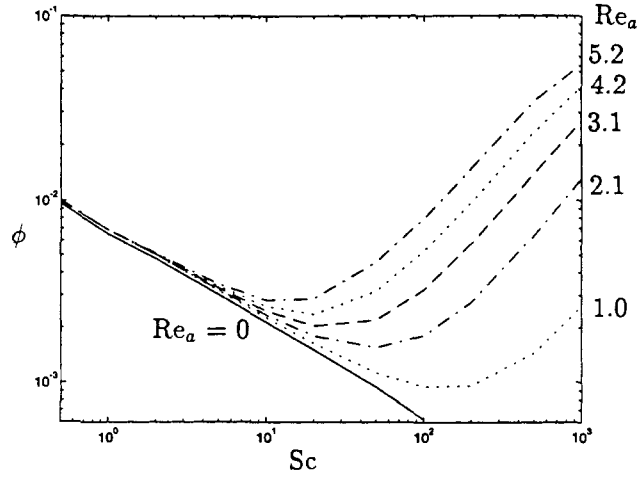

Figure 9. Axial dispersion vs. Schmidt number; the solid line is the result for $\bar{W} = 0$.

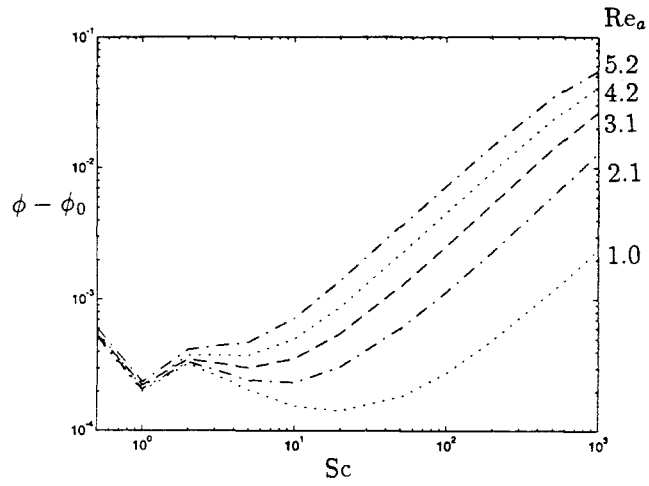

Figure 10. $\phi - \phi_0$ vs. Schmidt number.

The figure also shows the value for ϕ_0 calculated from Eq. 17 using $\alpha = 0.86$. The contribution to the axial dispersion due to molecular diffusion alone, $\phi = 1/(ReSc)$, is also shown in the figure. For $Sc = 0.5$, the axial dispersion exceeds the dispersion due to molecular diffusion by 20%, but when $Sc = 100$, the excess dispersion due to advection is 1,450%.

The effect on dispersion of varying the axial pressure gradient is shown in Figures 9 to 11. Figure 9 shows ϕ vs. Sc. The axial dispersion is increased due to the effect of axial flow. For low Schmidt numbers this increase is small, but for higher Schmidt numbers it becomes appreciable, especially when the axial flow rate is large. Figures 10 and 11 show $\phi - \phi_0$ for the flows, with Figure 10 showing the variation due to changing molecular diffusivity and Figure 11 showing the effect of increasing axial velocity (or equivalently increasing G) on the dispersion. Figure 10 shows that for $Sc > 50$ and $\bar{W} \geq 0.004$, the excess dispersion, $\phi - \phi_0$ is proportional to the Schmidt number and, for the same range of Schmidt number and axial flow rate, Figure 11 shows that $\phi - \phi_0$ is proportional to $\bar{W}^2$. As a result the true excess dispersion is proportional to $\bar{W}^2 d^2/D_m$. A best fit here gives $\phi \approx \phi_0 + 6.5 \times 10^{-4} \bar{W}^2 d^2/D_m$.

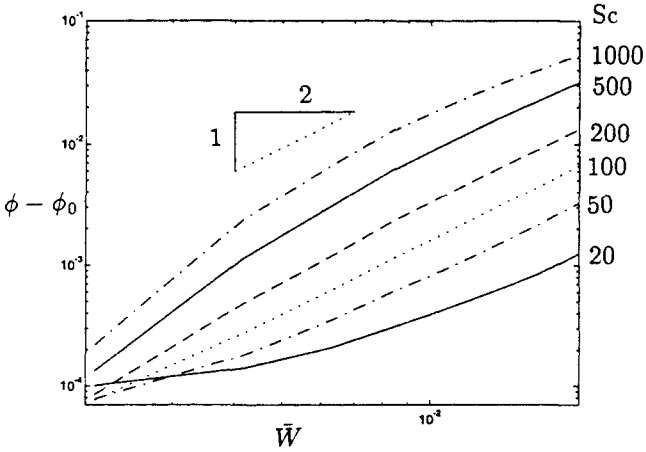

Figure 11. $\phi - \phi_0$ vs. axial velocity.

Discussion

The results of this study show that the method developed by Rosenbluth et al. (1987) gives a good estimate for the axial dispersion for laminar axisymmetric Taylor vortex flow where there is no superimposed axial flow. The results show that the effect of imposing an axial flow on the long-time dispersion of material in a Taylor vortex flow acts to increase the dispersion from that predicted for the same rotation but with no axial pressure gradient. This increase may be substantial, especially for situations where the axial flow is large and where the molecular diffusion of the material small. For example, as the axial flow Reynolds number increases from 0.5 to 5.0, dispersion at $Sc = 100$ increases by over one order of magnitude. The major contribution to the excess dispersion (on top of the dispersion expected for the case where there is no net flow) is due to the fact that the Taylor vortices are not moving with the net flow velocity, and as a result there is a countermoving stream of fluid, shown in Figures 4 and 6 as the dotted stream-function contour lines. This flow allows some global fluid communication to occur along the entire length of the annulus, although the cores of the vortices are still only able to communicate with the rest of the flow via molecular diffusion.

From these results, the dispersion shows a complex dependence on the molecular diffusion, with the dispersion due to the transport between vortices proportional to $\sqrt{D_m}$ and the added dispersion due to axial flow proportional to $1/D_m$. Moore and Cooney (1995) carried out a series of experiments to determine the axial dispersion in Taylor–Couette flow, and found no such dependence on molecular diffusion. In general they were looking at rotational rates an order of magnitude higher than those used in this study, where the flow would have broken down to wavy or turbulent Taylor–Couette flow.

Moore and Cooney also found that the dispersion that they measured was at least one order of magnitude greater than that predicted by Rosenbluth et al., even if a large value of $\hat{v} = \omega R_i$ is used for the roll velocity. They suggested that there was convective interchange across the vortex boundaries, possibly caused by the axial flow. The results of this study show that there is a further mechanism for axial dispersion in these flows—that caused by the difference in velocity between the vortex train and the mean flow.

The picture of Taylor vortices marching through the annulus as locally well-mixed units, but with overall plug flow, needs to be examined carefully, especially when the vortices do not move with the mean flow velocity. For a given Taylor number, as the vortex velocity increases, the excess dispersion also increases and the volume of fluid trapped within each vortex core decreases, reducing the size of each "reactor unit."

The method of Brenner (1980) has worked well for the conditions where the Schmidt number was less than about 100, and reasonably for Schmidt numbers of less than 1000. To explore the dispersion for higher Schmidt numbers, and also to look at the way that the dispersing cloud develops, a different approach using the dispersion of a cloud of particles must be used, where molecular diffusion is simulated using a random jump. This will be the focus of a future study.

Notation

D_a = axial dispersion, m^2/s
i = radial grid point
k = axial grid point
n = time-step counter
Q = axial volumetric flow rate, m^3/s
r = radial coordinate
R_o = outer cylinder radius, m
Re = rotation Reynolds number $\omega R_i d/\nu$
z = axial coordinate
∂r = mesh spacing in the radial direction
∂z = mesh spacing in the axial direction
λ = Taylor vortex wavelength, m
$\phi_0 = G = 0$ axial dispersion

Literature Cited

Amsden, A. A., and F. H. Harlow, "The SMAC Method: A Numerical Technique for Calculating Incompressible Fluid Flows," LASL Rep. LA-4370, Los Alamos, NM (1970).

Brenner, H., "Spatially Periodic Porous Media," *Philos. Trans. Roy. Soc.*, **297**, 81 (1980).

Bühler, K., and N. Polifke, "Dynamical Behaviour of Taylor Vortices with Superimposed Axial Flow," *Nonlinear Evolution of Spatio-Temporal Structures in Dissipative Continuous Systems*, F. H. Busse and L. Kramer, eds., Plenium, New York (1990).

Carbonell, R. G., and S. Whitaker, "Dispersion in Pulsed Systems—II Theoretical Developments for Passive Dispersion in Porous Media," *Chem. Eng. Sci.*, **38**, 1795 (1983).

Chandrasekhar, S., "The Hydrodynamic Stability of Viscid Flow Between Coaxial Cylinders," *Proc. Natl. Acad. Sci. USA*, **46**, 141 (1960).

Chandrasekhar, S., "The Stability of Spiral Flow Between Rotating Cylinders," *Proc. Roy. Soc. London A*, **265**, 188 (1962).

Datta, "Stability of Spiral Flow Between Concentric Circular Cylinders at Low Axial Reynolds Number," *J. Fluid Mech.*, **21**, 635 (1965).

DiPrima, R. C., "The Stability of a Viscous Fluid Between Rotating Cylinders with an Axial Flow," *J. Fluid Mech.*, **9**, 621 (1960).

DiPrima, R. C., and A. Pridor, "The Stability of Viscous Flow Between Rotating Concentric Cyliners with an Axial Flow," *Proc. R. Soc. London A*, **366**, 555 (1979).

Gu, Z. H., and T. Z. Fahidy, "Characteristics of Taylor Vortex Structure in Combined Axial and Rotating Flow," *Can. J. Chem. Eng.*, **63**, 710 (1985).

Gu, Z. H., and T. Z. Fahidy, "The Effect of Geometric Parameters on the Structure of Combined Axial and Taylor-Vortex Flow," *Can. J. Chem. Eng.*, **64**, 185 (1986).

Kataoka, K., H. Doi, T. Hongo, and M. Futagawa, "Ideal Plug-Flow Properties of Taylor Vortex Flow," *J. Chem. Eng. Japan*, **8**, 472 (1975).

Kataoka, K., and T. Takigawa, "Intermixing Over Cell Boundary Between Taylor Vortices," *AIChE J.*, **27**, 504 (1981).

Koschmeider, E. L., *Bénard Cells and Taylor Vortices*, Chap. 13, Sec. 1, Cambridge University Press, Cambridge (1993).

Leonard, B. P., "A Stable and Accurate Convective Modelling Procedure Based on Quadratic Upstream Interpolation," *Comp. Methods Appl. Mech. Eng.*, **19**, 59 (1979).

Li, Y., and M. Rudman, "Assessment of Higher-Order Upwind Schemes Incorporating FCT for Convection Dominated Problems," *Numer. Heat Transfer, Part B*, **27**, 1 (1995).

Moore, C. M. V., and C. L. Cooney, "Axial Dispersion in Taylor-Couette Flow," *AIChE J.*, **41**, 723 (1995).

Morton, D. E., M. J. Rudman, and J.-L. Liow, "Numerical Simulation of Splashing Phenomena," *Int. Conf. on Numerical Methods in Laminar and Turbulent Flow*, C. Taylor and P. Durbetaki, eds., Atlanta, GA (1995).

Pudjiono, P. I., N. S. Tavare, J. Garside, and K. D. P. Nigam, "Residence Time Distribution from a Continuous Couette Flow Device," *Chem. Eng. J.*, **48**, 101 (1992).

Rosenbluth, M. N., H. L. Berk, I. Doxas, and W. Horton, "Effective Diffusion in Laminar Convective Flows," *Phys. Fluids*, **30**, 2636 (1987).

Samson, S. S. Y., and S. P. Ayazi, "Residence Time Distribution in a

Rotary Flow-Through Device," *Ind. Chem. Eng. Symp. Ser. 140*, 191 (1996).
Simmers, D. A. and J. E. R. Coney, "Velocity Distributions in Taylor Vortex Flow with Imposed Laminar Axial Flow and Isothermal Surface Heat Transfer," *Int. J. Heat Fluid Flow*, **2** 85 (1980).
Synder, H. A., "Experiments on the Stability of Spiral Flow at Low Axial Reynolds Numbers," *Proc. Roy. Soc. London A*, **265** 198 (1962).
Taylor, G. I., "Stability of a Viscous Liquid Contained Between Two Rotating Cylinders," *Philos. Trans. R. Soc. A*, **223**, 289 (1923).
Welch, J. E., F. H. Harlow, J. P. Shannon, and B. J. Daly, "The MAC Method. A Computing Technique for Solving Viscous, Incompressible, Transient Fluid-Flow Problems Involving Free Surfaces," LASL Rep. LA-3425, Los Alamos, NM (1965).
Zalesak, S. T., "Fully Multidimensional Flux-Corrected Transport Algorithms for Fluids," *J. Comput. Phys.*, **31**, 335 (1979).

Manuscript received Mar. 3, 1997, and revision received Sept. 22, 1997.